 FDMP, vol.11, no.2, pp.127-142, 2015

Parametric Study of Bubble Kinematic Behaviour in a Centrifugal Vacuum Separator

Yuan Chen[1], Honggang Duan[1], Fei Yu[1], Xingyu Zhao[1], Han Xu[1], Jun Gao[1,2]

Abstract: The dynamics of dispersed bubbles in a centrifugal separator are investigated with the aim to improve the efficiency of the system. The prototype separator consists of a rotor, a base, a diverting disc, a shaft, an oil trapping impeller, a central pipe, an inlet section for contaminated oil, an outlet section for purified oil and an air outlet. A hydrodynamic model is developed to predict the complex influence of parameters such as the centrifugal force and vacuum pressure. In particular, three different force models are selected to analyze the effect of the added mass and Basset forces (also including inertia, and the buoyancy and drag forces). The bubble kinematic behaviour is simulated in detail by using a discrete-phase numerical method. Results show that gas concentration and vacuum pressure can significantly influence the removal of bubbles.

Keywords: bubble, bubble kinematic behaviour, gas–liquid–solid separator, contaminated oil

1 Introduction

Contaminants in hydraulic oil accelerate the wear of machine components [Bertel et al. (2011)]. These contaminants exist in many types, such as solid particulate, water, and air. Gravitational separation, centrifugal separation, impingement, and filters are four types of physical separation techniques [Nicolus et al. (2013); Galvin and Dickinson (2013); Francesc and Ricard (2013)]. Centrifugal separation is able to remove solid particulates and high-density water, but cannot extract dissolved air and low-density water. Unlike other basic separation techniques, the centrifugal vacuum gas–liquid–solid separator proposed in [Hu and Liu (2013)] can not only remove free water and solid particulates greater than 2 μm in diameter, but also extract dissolved air and water because of vacuum pressure.

[1] Shandong University at Weihai, Weihai, China
[2] Corresponding Author. Email: shdgj@sdu.edu.cn

The presence of bubbles in viscous fluid causes excessive oxidation, cavitation, and decrease of film strength [Cui et al. (2012)]. The gas–liquid–solid separator is often operated in the bubbling regime subject to complicated change of centrifugal force and vacuum pressure. In such system, the bubble kinematic behaviour is mainly dependent on the bubble physical properties (represented by modelling parameters) and the operating parameters of the separator (e.g., rotating speed and vacuum pressure). Over the past two decades, many studies have focused on understanding the effects of various physical properties (e.g. viscosity [Chen and Guo (2014); Hajizadeh-Aghdam et al. (2012)], interface contamination [Huang et al. (2012)], surfactant [Hayashi and Tomiyama (2012)], viscoelasticity [Lind and Phillips (2010)], and surface tension [Ehsan et al. (2011)]) on bubble kinematic behaviour under atmospheric pressure. However, detailed information is still unavailable regarding the effects of operating parameters on bubble kinematic behaviour under vacuum pressure. With the presence of centrifugal force and vacuum pressure, bubbles in the gas–liquid–solid separator exhibit both a rising motion along the vertical direction and a circular motion around the centre of the separator. The combination of these two motions of the bubbles, or their composite motion, generates turbulent flow and accounts for their complex kinematic behaviours. Therefore, a detailed numerical simulation of bubble kinematic behaviour (i.e., velocity, shape, and motion trajectory) in the gas–liquid–solid separator is essential to elucidate the influence of modelling and operating parameters. Previous research on this topic has mainly focused on the collision between bubbles [Martin et al. (2013); Sungkorn et al. (2014)], the rising behaviour of a single bubble [Zuo et al. (2013); Bu and Zhao (2012)], bubble shape and formation [Zhang et al. (2012); He et al. (2013)], and bubble dynamics [Liu et al. (2013); Szewc et al. (2013)]. To the best of our knowledge, no study has investigated the composite motion of bubbles in contaminated oil.

In the present study, detailed discrete numerical method is used to investigate the effects of modelling and operating parameters on bubble kinematic behaviour subject to centrifugal force and vacuum pressure. The objective of the study is to provide insight into the improvement of bubble purification efficiency of the gas–liquid–solid separator. The rest of the paper is organised as follows. The hydrodynamic model of bubble is presented in Section 2. Simulation results are discussed in Section 3 and the conclusion is given in Section 4.

2 Hydrodynamic model of bubble

Figure 1 shows the diagram of a centrifugal vacuum gas–liquid–solid separator proposed in [Hu and Liu (2013)]. The separator can not only remove solid particulates and free water, but also extract dissolved air and water. The prototype of the sep-

arator consists of the following parts: rotor (1), base (2), diverting disc (3), shaft (4), impeller trapping oil (5), central pipe (6), inlet of contaminated oil (7), outlet of purified oil (8) and air outlet (9).

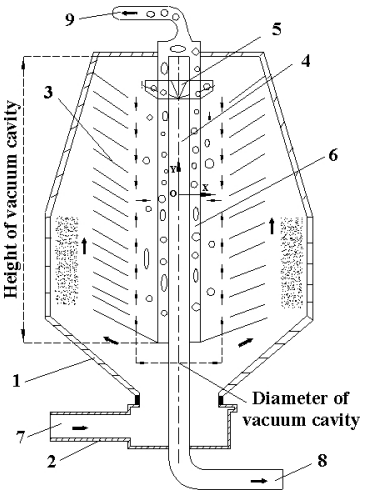

Figure 1: Diagram of the prototype of a centrifugal vacuum separator

As shown in Figure 1, the shaft is located at the center of the filter cylinder, and the impeller trapping oil sits on the shaft. The discs diverting the oil are fixed onto the rotor. When the rotor rotates at a high speed, a vacuum cavity in the rotor is built around the shaft. The central pipe with air outlet is installed in the inner cavity of the shaft, and a vacuum pump is connected to the air outlet. All the gas chambers connected to the central pipe are evacuated by the vacuum pump. When the rotor rotates at a high speed, the contaminated oil in the separator is moved away from the axis by strong centrifugal force. Solid particulates and free water, the density of which is greater than that of the oil, are thrown onto the inner wall of the rotor. However, the dissolved air and water with low density approach the vacuum cavity in the rotor before being discharged from the air outlet by vacuum pump. The separation of bubble from solid particulate dramatically reduces their collision. Therefore, the collision behaviour between bubble and solid particulate can be neglected in bubble kinematic model while ensuring the accuracy of the model. The direction of airflow is indicated by an arrow, and the coordinate system is presented in Figure 1.

2.1 Hydrodynamic equation of bubbles in contaminated oil

In this paper, the fluid is assumed to be isothermal, and collisions between two bubbles are neglected. Thus, each individual bubble is treated as a single particle

with three degrees of freedom. According to Newton's kinematic equation, the force balance equation of a spherical bubble can be expressed as follows:

$$\begin{cases} \rho_b V_b \dfrac{du_h}{dt} = F_w + F_d \\ \rho_b V_b \dfrac{du_v}{dt} = F_g + F_b + F_d + F_{am} + F_{ba} \end{cases} \tag{1}$$

where ρ_b, V_b, u_v, and u_h represent the density, volume, vertical velocity, and horizontal velocity of bubble, respectively. The terms on the right-hand side are the contributions of different forces, including inertial force (F_g), buoyancy force (F_b), drag force (F_d), added mass force (F_{am}), Basset force (F_{ba}), and centrifugal force (F_w). The term on the left-hand side represents the inertia of the bubble.

The sum of gravity and buoyancy forces (F_g +F_b), drag force (F_d), added mass force (F_{am}), and Basset force (F_{ba}) can be expressed as follows [Magnaudet and Eames (2000)]:

$$\begin{cases} F_g + F_b = (\rho_f - \rho_b) V_b g \\ F_d = -\dfrac{1}{2} C_D \rho_f \pi R_b^2 \left| u_b - u \right| (u_b - u) \\ F_{am} = -\dfrac{1}{2} \rho_f V_b \left(\dfrac{du_b}{dt} - \dfrac{du}{dt} \right) \\ F_{ba} = -3\pi\eta D_b \displaystyle\int_0^t \kappa(t-\tau) \frac{d(u_b - u)}{dt} d\tau \end{cases} \tag{2}$$

where the vector $u_b - u$ denotes the relative velocity between bubble and contaminated oil; the drag coefficient C_D is a function of bubble Reynolds number R_e, and its value is examined in detail in Section 3.2; the kernel $\kappa(t-\tau)$ is a function that expresses the importance of past accelerations on the actual Basset force; η is the kinematic viscosity of contaminated oil; D_b denotes the bubble diameter; and R_b is the bubble radius.

Substituting Eq. (2) into the force balance Eq. (1) yields the following equation:

$$\begin{cases} \dfrac{du_h}{dt} = \dfrac{\rho_f - \rho_b}{\rho_b} \omega^2 r - 0.5 \dfrac{C_D \rho_f \pi R_b^2 u_h^2}{\rho_b \left(\frac{4}{3} \pi R_b^3 \right)} \\ \dfrac{du_v}{dt} = \dfrac{1}{(\rho_b + 0.5\rho_f) V_b} \left[\begin{array}{l} (\rho_f - \rho_b) V_b g - \dfrac{1}{2} C_D \rho_f \pi R_b^2 \\ |u_v - u| \cdot (u_v - u) - D_b^2 \sqrt{\pi \rho_f \mu} \cdot \\ \displaystyle\int_0^t \frac{1}{\sqrt{t-\tau}} \frac{du_v}{dt} d\tau \end{array} \right] \end{cases} \tag{3}$$

where R_b, ω, and r represent the bubble radius, centrifugal angular velocity, and distance between bubble and center of the rotor, respectively; u_v and u_h are the vertical and horizontal velocities of bubble, respectively.

2.2 Mass transfer between bubble and contaminated oil

The mass transfer rate of each bubble can be calculated as follows:

$$\frac{dn}{dt} = \frac{2\pi R_b}{29} \cdot Sh \cdot D_{AB} \cdot (C_A - C_I) \tag{4}$$

In Equation (4), C_A, represents the concentration of dissoluble gas inside the bubble ($C_A = H \cdot P$, where H is Henry's constant and P is the total pressure inside bubble); C_I is the concentration of dissoluble gas in the contaminated oil surrounding the bubble; D_{AB} is the molecular diffusion coefficient; n denotes the molar amount of gas inside the bubble; and Sh is the Sherwood number. The Sherwood number is equal to $1 + Sc^{1/3}(1 + 1/Re \cdot Sc)^{1/3} \cdot Re^{0.41}$, where $Sc = \eta / D_{AB}$ [Clift, Grace and Weber (1978)].

In the gas–liquid–solid separator, the total pressure inside the bubble is the sum of the vacuum pressure and the pressure related to centrifugal acceleration and surface tension. Thus, it can be expressed as follows:

$$P = P_0 + \frac{4}{3} R_b (\rho_f - \rho_b) \omega^2 r + 2\sigma / R_b \tag{5}$$

where P_0 is the vacuum negative pressure and σ is the surface tension coefficient. In Equation (5), the second term on the right-hand side represents the pressure caused by centrifugal acceleration, and the third term is the pressure due to surface tension;

The rate of pressure change inside the bubble can be obtained using the first derivative of Eq. (5) with respect to time:

$$\frac{dP}{dt} = \frac{4}{3} (\rho_f - \rho_b) \omega^2 \left[r \frac{dR_b}{dt} + R_b \frac{dr}{dt} \right] - \frac{2\sigma}{R_b^2} \frac{dR_b}{dt} \tag{6}$$

The rate of gas mole change inside the bubble can be calculated from the state equation of ideal gas ($PV = nRT$):

$$RT \frac{dn}{dt} = \frac{4}{3} \pi R_b^3 \frac{dP}{dt} + 4\pi R_b^2 P \frac{dR_b}{dt} \tag{7}$$

Substituting Eqs. (4) and (6) into Eq. (7) yields the rate of the change in bubble radius:

$$\frac{dR_b}{dt} = \frac{RT \dfrac{dn}{dt} - \dfrac{16}{9} \pi R_b^4 (\rho_f - \rho_b) \omega^2 \dfrac{dr}{dt}}{\dfrac{16}{9} \pi R_b^3 (\rho_f - \rho_b) \omega^2 r - \dfrac{8}{3} \pi R_b \sigma + 4\pi R_b^2 P} \tag{8}$$

3 Results and discussions

In this section, various numerical simulations are performed to study the effects of modeling and operating parameters (e.g., drag coefficient, dissoluble gas concentration in the contaminated oil, centrifugal angular velocity, and vacuum negative pressure) on bubble kinematic behaviour in the separator. The modeling parameters related to bubble physical properties include drag coefficient and the concentration of dissoluble gas in contaminated oil. Likewise, the operating parameters of the separator are composed of centrifugal angular velocity and vacuum pressure. The simulation can be performed numerically using subroutine ODE45 of MATLAB software. The time step of bubble simulation is selected as 5×10^{-6} s. A number of spherical bubbles are positioned in flowing contaminated oil with an average flow velocity of 0.4547 m/s, and these bubbles move at a complex composite motion trajectory. The contaminated oil is assumed to be incompressible, isothermal, and to have constant physical properties. The values of physical properties of gas and contaminated oil are selected as follows: bubble and oil density ($\rho_b = 1.29$ kg/m^3, $\rho_f = 878$ kg/m^3), kinematic viscosity of oil ($\eta = 46$ mm$^2/s$), surface tension coefficient of bubble ($\sigma = 0.036$ N/m), molecular diffusion coefficient ($D_{AB} = 0.181 \times 10^{-4}$ m^2/s), Henry's constant ($H = 0.0093$ mol/(m^3·Pa)), universal gas constant ($R = 8.314$ J/(mol·K)) and concentration of dissoluble gas in oil ($C_A = 4.1636$ mol/m^3).

3.1 Prediction of Bubble Kinematic Behavior using Different Models

The prediction of bubble kinematic behaviour varies depending on different forces applied. Three force models are selected for the numerical equations to analyze the effect of the added mass and Basset forces. In the first model, the momentum balance in Eq. (1) does not include either the added mass or Basset forces. The second model contains the added mass force but not the Basset force, while the third model includes both.

Figure 2 illustrates the velocities and radii of bubbles calculated by the above three force models. As shown in Fig. 2(a), the vertical velocities in the second force model are approximately equal to those in the third force model, showing that Basset force has minimal effect on the vertical velocities of bubbles. However, significant differences can be found in the vertical velocities between the first and third force models, suggesting that the added mass force significantly affects the vertical velocities. The influence of the three force models on the horizontal velocities is also shown in Fig. 2(b), which indicates that the added mass force strongly affects the horizontal velocities. For convenience, the relative influence of added mass/Basset force on the horizontal velocities is defined

as $\Delta u_h(F_{am}$ or $F_{ba})/u_h(F_g,F_b,F_d,F_{am},F_{ba})$, where $\Delta u_h(F_{am}$ or $F_{ba})$ denotes the absolute influence of the added mass/Basset force on the horizontal velocities, and $u_h(F_g,F_b,F_d,F_{am},F_{ba})$ represent the horizontal velocity. The relative influence of the added mass and Basset forces are calculated as 81.143% and 0.895%, respectively. Due to its small influence, the Basset force can be neglected in the momentum equation (Eq. (1)).

As shown in Fig. 2(c), the radius of the bubble in the second force model is the same as that in the third force model. However, a minimal difference can be observed between the first force model and the other two models. The relative influence of the added mass and Basset forces on the bubble radius are approximately 0.80615% and 0.20693%, respectively. Compared with Basset force, the added mass force has a greater influence on the kinematic behaviour of bubbles. Therefore, in the hydrodynamic equation the added-mass force should be considered while the Basset force can be reasonably neglected.

3.2 Effects of Modeling parameters on bubble kinematic behaviour

The modeling parameters related to bubble physical properties, such as drag coefficient and dissoluble gas concentration in the contaminated oil, influence the kinematic behaviours of bubbles.

3.2.1 Effects of drag coefficient in contaminated oil

The drag coefficient C_D in Eq. (2) is a function of the bubble Reynolds number R_e. A general correlation for the drag coefficient of a particle in contaminated liquid was proposed by Turton and Levenspiel [Turton and Levenspiel (1986)]. This correlation is applicable for rigid bubbles with $R_e < 130$:

$$C_D = \frac{24}{R_e}\left(1+0.173R_e^{0.667}\right) + \frac{0.413}{1+16300R_e^{-1.09}} \text{ for } R_e < 130 \tag{9}$$

where $R_e = \rho_f D_b|u_b - u|/\mu$.

Another general correlation for the drag coefficient of a rigid spherical particle was proposed by Schiller and Nauman [Schiller and Nauman (1935)], and this correlation can be expressed as follows:

$$C_D = \begin{cases} \dfrac{24}{R_e}\left(1+0.15R_e^{0.687}\right), & R_e \le 1000 \\ 0.44, & R_e > 1000 \end{cases} \tag{10}$$

For bubble swarms in viscous Newtonian liquids, the correlation proposed by Laín

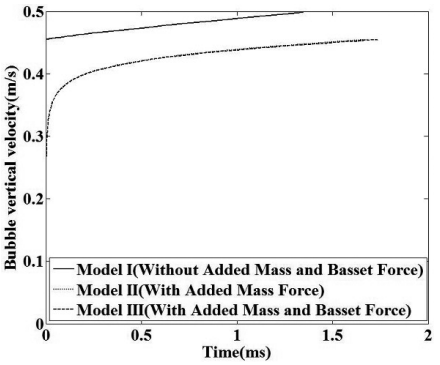

(a) bubble vertical velocity

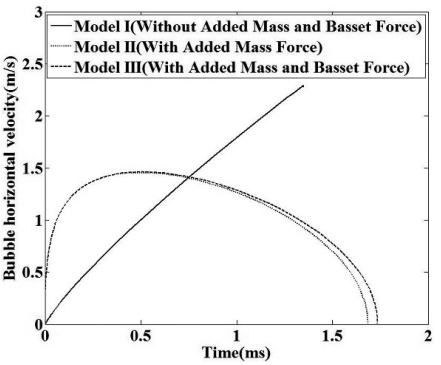

(b) bubble horizontal velocity

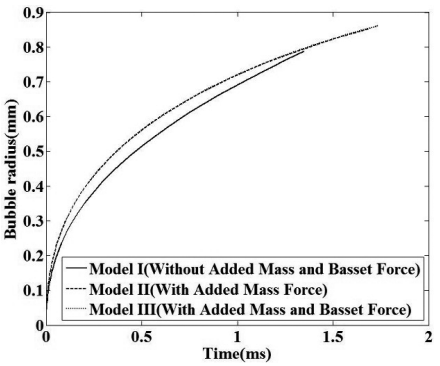

(c) bubble radius

Figure 2: Bubble velocities and radii by different force models ($R_b = 10$ um)

has excellent agreement with the experimental data [Laín et al. (2002)].

$$C_D = \begin{cases} 16R_e^{-1}, & R_e < 1.5 \\ 14.9R_e^{-0.78}, & 1.5 < R_e < 80 \\ 48R_e^{-1}\left(1 - 2.21R_e^{-0.5}\right) + 1.86 \times 10^{-15}R_e^{4.756}, & 80 < R_e < 1500 \\ 2.61, & 1500 < R_e \end{cases} \tag{11}$$

Mei [Mei and Adrian (1992)] proposed the following correlation for the drag coefficient of the bubble with mobile surface in liquid without contaminants.

$$C_D = \frac{16}{R_e}\left[1 + \left\{\frac{8}{R_e} + \frac{1}{2}\left(1 + \frac{3.315}{R_e^{0.5}}\right)\right\}^{-1}\right] \tag{12}$$

The drag force of bubble in liquid is largely dependent on the presence of surface-active contaminants. For bubbles in liquid without contaminants, the liquid exerts

no shear force on the bubble surface, and the interface between the bubbles and liquid is mobile. Thus, smaller value of the drag coefficient in Eqs. (11) and (12) is appropriate for such bubbles. In contrast, the bubbles in liquid with contaminants have a non-zero shear stress, and the drag coefficient is greater than that in clean liquid. The interface between the bubbles and the liquid is immobilized to a certain extent. Magnaudet and Eames [Magnaudet and Eames (2000)] demonstrated that the drag coefficient of a bubble in contaminated liquid can be accurately approximated by the behaviour of a solid particle under no-slip boundary condition. This means that it is suitable to apply the drag coefficients in Eqs. (9) and (10) to bubbles in contaminated liquid.

Numerical simulations of bubble rising in water are conducted to validate the decision-making approach through which the value of drag coefficient is obtained. The simulation results are illustrated in Fig. 3. As shown in Fig. 3(a), the vertical velocities computed from the drag coefficients in Eqs. (9) and (10) are approximately equal to the data previously reported [Bergman (1958)]. The relative difference between the simulation and experimental data is approximately 23 %. The vertical velocities corresponding to the drag coefficient in Eq. (11) are approximately equal to those computed from the drag coefficient in Eq. (12). However, a relative difference ad large as 56 % exists between the present simulation and the experimental data in reference [Bergman (1958)]. Accordingly, the drag coefficients in Eqs. (9) and (10) are more suitable to bubbles in liquid without contaminants.

Contaminated oil contains surface active contaminants, such as solids, gas, and water. Thus, Eq. (11) or (12) is selected to determine the drag coefficient C_D in this paper. Figs. 3(b) and 3(c) show the simulation results of the bubble kinematic behaviour in the separator. As shown in Figs. 3(b) and 3(c), the drag coefficient has greater influence on the horizontal velocity than on the vertical velocity. This is mainly because of the large drag force along the horizontal direction caused by the centrifugal force.

3.2.2 Effects of dissoluble gas concentration in contaminated oil

The gas content in contaminated oil affects air purification in the separator. The mass transfer equation (Eq. (4)) shows that if the gas content in the contaminated oil is greater than the dissoluble gas content inside a bubble, the gas molecules in the contaminated oil will be transferred into the bubble, which enlarges the radius of the bubble. Otherwise, the bubble radius will decrease. Figure 4 illustrates the influence of different C_A on the kinematic behaviour of bubbles.

As shown in Figs. 4(a) and 4(b), the concentration of the dissoluble gas in contaminated oil has greater influence on the horizontal velocity than on the vertical velocity, because the increase in bubble radius caused by dissoluble gas concentra-

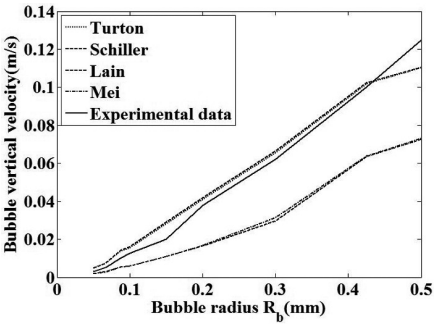

(a) relation between the vertical velocity and the bubble radius

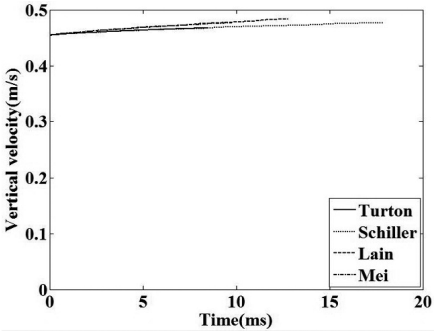

(b) variation law of the vertical velocity

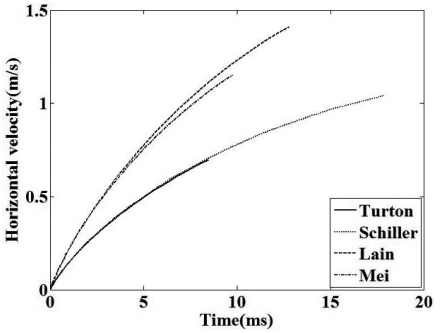

(c) variation law of the horizontal velocity

Figure 3: Kinematic behaviour of bubbles with different drag coefficients

tion does not significantly increase the centrifugal force. As shown in Fig. 4(c), the concentration value C_A also significantly influences the bubble radius. The rate of relative change in bubble radius from $C_A/2$ to $C_A/4$ can be calculated as $\Delta R_b(C_A/2, C_A/4)/R_b(C_A/4) = 13.5\%$. Thus, a smaller concentration corresponds to an easier removal of the bubble from the separator [Fig. 4(d)].

3.3 Effects of operating parameters on bubble kinematic behaviour

Operating parameters of the separator also influence the bubble kinematic behaviours. These operating parameters include the centrifugal angular velocity and the vacuum negative pressure. The centrifugal angular velocity is involved in the movement of bubbles toward the center of the vacuum cavity. The bubbles are then removed from the separator by the vacuum pressure. Fig. 5 shows the numerical simulation results of the kinematic behaviour of a bubble with a radius of 0.5 μm at centrifugal angular velocities of $\omega = 4000$, 6000, 8000 r/min. The centrifugal angular velocity influences both the velocity and the radius of the bubble. As shown in Figs. 5(a)

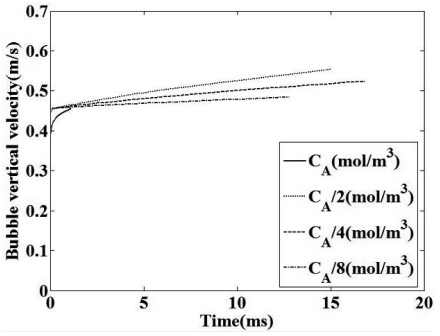

(a) bubble vertical velocity

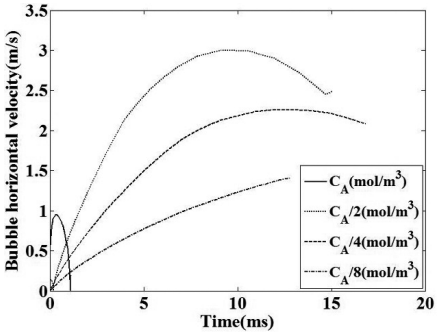

(b) bubble horizontal velocity

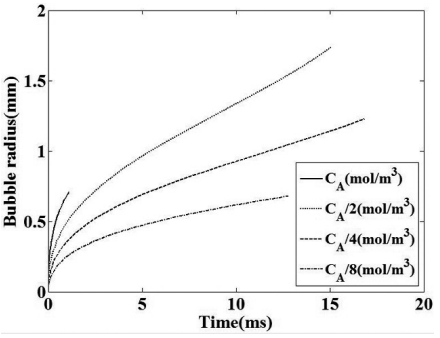

(c) bubble radius

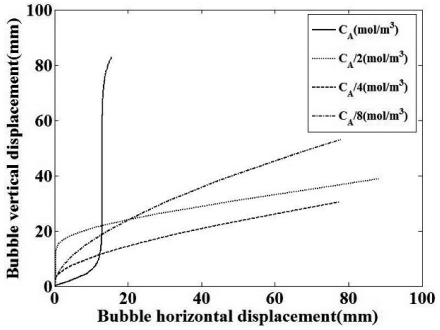

(d) motion trajectory

Figure 4: Kinematic behaviour of bubbles with different concentrations of dissoluble gas in contaminated oil

and 5(b), an increase in angular velocity results in the rise of the horizontal velocity of a bubble but exerts insignificant influence on the vertical velocity. Thus, a larger centrifugal velocity corresponds to an easier removal of the bubble from the separator [Fig. 5(d)].

The minimum radii of the bubble, which can be separated from the gas–liquid–solid separator, are calculated as 0.233, 0.237, 0.246, 0.261, and 0.289 μm at centrifugal angular velocities of 8000, 7000, 6000, 5000, 4000 r/min, respectively. The simulation results are in good agreement with the theoretical analysis stating that larger centrifugal angular velocity can efficiently separate bubbles with smaller radii from the separator. However, the differences among the minimum radii are so small that they are negligible. Therefore, the centrifugal angular velocity within the given range has small influence on the kinematic behaviour of bubble.

The vacuum pressure also contributes to extracting the bubbles from the separator. A certain generalization can be derived from Eq. (4) and Henry's law. The vacuum pressure affects the bubble radius and its kinematic behaviour by changing the

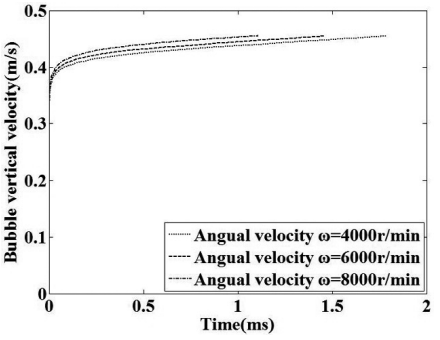

(a) bubble vertical velocity

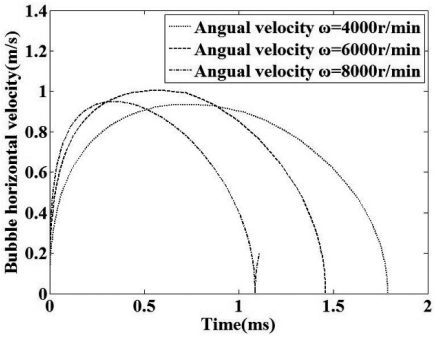

(b) bubble horizontal velocity

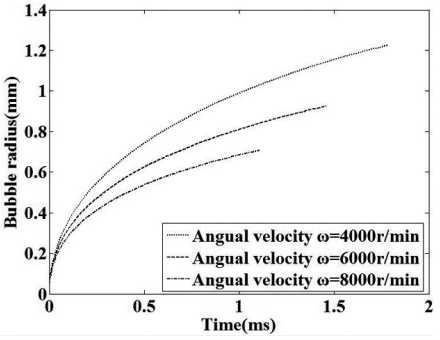

(c) bubble radius

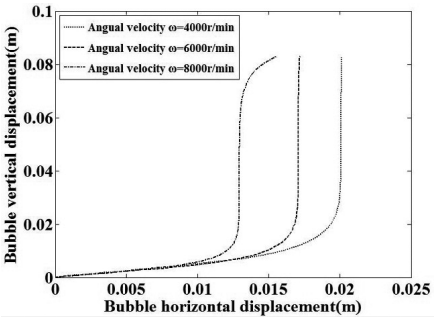

(d) motion trajectory

Figure 5: Kinematic behavior of bubbles with different centrifugal angular velocities in the gas–liquid–solid separator

concentration of the dissoluble gas inside the bubble. Fig. 6 shows the kinematic behaviour of a bubble at vacuum pressure of 9.5, 7.5, and 5.5 KPa. As shown in Figs. 6(a) and 6(b), the vacuum pressure has greater influence on the horizontal velocity than on the vertical velocity, and a lower vacuum pressure can extract the bubbles more easily from the separator. However, the determination of the vacuum pressure is related to the working environment and the device.

4 Conclusion

Mathematical models have been developed to investigate the bubble kinematic behaviour in a centrifugal vacuum separator by integrating interphase interaction forces, including inertia force, buoyancy force, drag force, added mass force, and Basset force, into Newtonian kinematic equations. A comprehensive numerical study of bubble kinematic behaviour in the gas-liquid-solid separator under the complex actions of centrifugal force and vacuum negative pressure has been conducted

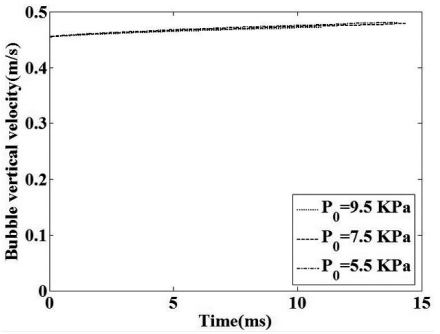

(a) bubble vertical velocity

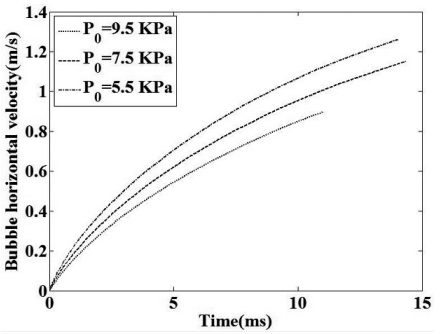

(b) bubble horizontal velocity

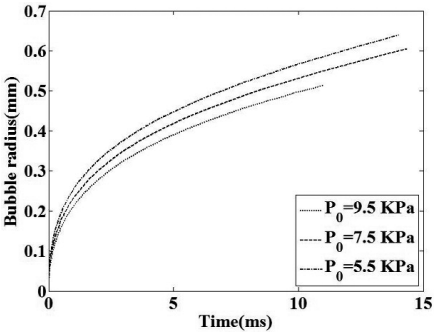

(c) bubble radius

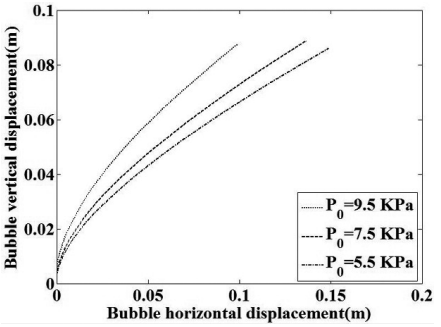

(d) motion trajectory

Figure 6: Kinematic behaviors of a bubble under different atmospheric pressure in the gas–liquid–solid separator

by using discrete phase numerical method.

Comparative simulations based on three force models have demonstrated that the added mass force is not negligible for the accelerated motion of bubbles, whereas Basset forces can be neglected.

The main outcomes of the numerical study can be summarized as follows. First, large values of drag coefficients are suitable for the bubbles in contaminated oil because of the surface active contaminants. Second, a smaller concentration of dissoluble gas in the contaminated oil corresponds to an easier removal of bubbles from the separator. Third, a centrifugal angular velocity within the given range has minimal effects on the kinematic behaviour of bubbles. Fourth, a low vacuum pressure helps to extract the bubbles, and the bubble minimum radius is inversely proportional to the vacuum pressure. Future work shall be devoted to define a precise feed flow rate.

Acknowledgement: This project is supported by National Natural Science Foundation of China (Grant No. 51375264), China Post-doctoral Science Foundation (Grant No. 2014T70632 and 2013M530318), and Research Awards Fund for Excellent Young and Middle-aged Scientists of Shandong Province (Grant No. BS2013ZZ008) and Post-doctoral innovation funds of Shandong Province (Grant No. 201303105).

References

Bergman, P.G. (1958):*Physics of sound in the sea*. Beijing:Science Press.

Bertel, N.; Dimitra, T.; Maciej, J.; Tomasz, K.; William, S.; Knud, E. K. (2011): Combining steam injection with hydraulic fracturing for the in situ remediation of the unsaturated zone of a fractured soil polluted by jet fuel. *Journal of Environmental Management*, vol. 92, no. 3, pp. 695-707.

Bu, L.; Zhao, J.Y. (2012): Numerical simulation of the water bubble rising in a liquid column using the combination of level set and moving mesh methods in the collocated grids. *International Journal of Thermal Sciences*, vol.59, pp. 1-8.

Chen, S. L.; Guo, L. J. (2014): Viscosity Effect on regular bubble entrapment during drop impact into a deep pool. *Chemical Engineering Science*, vol. 109, pp. 1-16.

Clift, R.; Grace, J.R.; Weber, M.E. (1978): *Bubbles, Drops and Particles*. Academic Press, New York, 1978: 26-121.

Cui, Y.; Gao, H.; Sun, J. S.; Wang, Y.H.; Chen, X.; Jiang, S. (2012): Numerical simulation of gas–solid flow in a conveying vessel. *Powder Technology*, vol. 226, pp. 34-42.

Ehsan, S.; Mehrzad, S.; Reza, E. (2011): A novel numerical scheme for the investigation of surface tension effects on growth and collapse stages of cavitation bubbles. *European Journal of Mechanics B/Fluids*, vol.30, pp.41-50.

Francesc, S.; Ricard, G. C. (2013): Effects of momentum flux and separation distance on bubbly jet impingement in microgravity conditions. *Chemical Engineering Science*, vol. 97, no. 28, pp. 272-281.

Galvin, K.P.; Dickinson, J.E. (2013): Particle transport and separation in inclined channels subject to centrifugalforces. *Chemical Engineering Science*, vol. 87, no. 14, pp. 294-305.

Hajizadeh-Aghdam, A.; Ohl, S.W.; Khoo, B.C.; Shervani-Tabar, M.T. (2012): Effect of the viscosity on the behavior of a single bubble near a membrane. *International Journal of Multiphase Flow*, vol. 47, pp. 17-24.

Hayashi, K.; Tomiyama, A. (2012): Effects of surfactant on terminal velocity of a Taylor bubble in a vertical pipe. *International Journal of Multiphase Flow*, vol.39, pp. 78-87.

He, J. F.; Zhao, Y.M.; Luo, Z.F.; He, Y.Q.; Duan, C.L. (2013): Numerical simulation and experimental verification of bubble size distribution in an air dense medium fluidized bed. *International Journal of Mining Science and Technology*, vol. 23, pp.387-393.

Hu, Y.L.; Liu, P. (2013): Centrifugal vacuum gas-liquid-solid separator, *China Patent CN103111099*, 2013.

Huang, Z.; Legendre, D.; Guiraudc, P. (2012): Effect of interface contamination on particle–bubble collision. *Chemical Engineering Science*, vol. 68, pp. 1-18.

Laín, S.; Bröder, D.; Sommerfeld, M.; Göz, M.F. (2002): Modelling hydrodynamics and turbulence in a bubble column using the Euler-Lagrange procedure. *Int.J. Multiphase Flow*, vol. 28, pp. 1381-1407.

Lind, S.J.; Phillips, T.N. (2010): The effect of viscoelasticity on a rising gas bubble. *Journal of Non-Newtonian Fluid Mechanics*, vol. 165, pp. 852-865.

Liu, J.R.; Zhu, C.Y.; Fu, T.T.; Ma, Y.G.; Li, H.Z. (2013): Numerical simulation of the interactions between three equal-interval parallel bubbles rising in non-Newtonian fluids. *Chemical Engineering Science*, vol.93, pp. 55-66.

Magnaudet, J.; Eames, I. (2000): The motion of high-Reynolds-Number bubbles in inhomogeneous flows. *Annual Review of Fluid Mechanics*, vol. 32, pp. 659-708.

Martin, H.; Pavlína, B.; Jiří, V. (2013): Collision of a small rising bubble with a large falling particle. *International Journal of Mineral Processing*, vol. 121, no. 10, pp. 21-30.

Mei, R.W.; Adrian, R.J. (1992): Flow Past a Sphere with an Oscillation in the Free-Stream Velocity and Unsteady Drag at Finite Reynolds Number. *Journal of Fluid Mechanics*, vol. 237, pp. 323-341.

Nicolus, R.; Ritva, T.; Marjatta, L.K. (2013): Modeling and simulation of gravitational solid–solid separation for optimum performance. *Powder Technology*, vol. 239, pp. 337-347.

Schiller, L.; Nauman, Z. (1935): *A drag coefficient correlation*. Z. Ver. Deutsch. Ing., vol. 77, pp.318-322.

Sungkorn, R.; Derksen, J.J.; Khinast, J.G. (2011): Modeling of turbulent gas-liquid bubbly flows using stochastic Lagrangian model and lattice-Boltzmann scheme. *Chemical Engineering Science*, vol.66, no.12, pp. 2745-2757.

Szewc, K.; Pozorski, J.; Minier, J.P. (2013): Simulations of single bubbles rising through viscous liquids using Smoothed Particle Hydrodynamics. *International Journal of Multiphase Flow*, vol.50, pp. 98-105.

Turton, R.; Levenspiel, O. (1986): A short note on the drag correlation for spheres. *Powder Technology*, vol. 47, no. 1, pp. 83-86.

Zhang, Y.J.; Liu, M.Y.; Xu, Y.G.; Tang, C. (2012): Three-dimensional volume of fluid simulations on bubble formation and dynamics in bubble columns. *Chemical Engineering Science*, vol. 73, pp. 55-78.

Zuo, J.L.; Tian, W.X.; Chen, R.H.; Qiu, S.Z.; Su, G. H. (2013): Two-dimensional numerical simulation of single bubble rising behavior in liquid metal using moving particle semi-implicit method. *Progress in Nuclear Energy*, vol. 64, pp. 31-40.